PCCP

Accepted Manuscript

ROYAL SOCIETY OF CHEMISTRY

www.rsc.org/pccp

Effect of H bond removal and changes in the position of the iron-sulphur head domain on spin-lattice relaxation properties of $[2Fe\text{-}2S]^{2+}$ Rieske cluster in cytochrome bc_1

Marcin Sarewicz, Małgorzata Dutka, Rafał Pietras, Arkadiusz Borek and Artur Osyczka*

Department of Molecular Biophysics, Faculty of Biochemistry, Biophysics and Biotechnology, Jagiellonian University, Kraków, Poland

*Corresponding author: artur.osyczka@uj.edu.pl, telephone: +48 12 664 63 48

Here, comparative electron spin-lattice relaxation studies of the 2Fe-2S iron-sulphur (Fe-S) cluster embedded in a large membrane protein complex – cytochrome bc_1 – are reported. Structural modifications of the local environment alone (mutations S158A and Y160W removing specific H bonds between Fe-S and amino acid side chains) or in combination with changes in global protein conformation (mutations/inhibitors changing the position of the Fe-S binding domain within the protein complex) resulted in different redox potential as well as *g*-, *g*-strain and the relaxation rates (T_1^{-1}) for the Fe-S cluster. The relaxation rates for T < 25 K were measured directly by inversion recovery while for T > 60 K they were deduced from simulation of continuous wave EPR spectra of the cluster with a model that included anisotropy of Lorentzian broadening. In all cases, the relaxation rate involved contributions from direct, second-order Raman and Orbach processes, each dominating at different temperature ranges. The analysis of T_1^{-1} (T) over the range 5-120 K yielded the values of the Orbach energy (E_{Orb}), Debye temperature θ_D and Raman process efficiency C_{Ram} for each variants of the protein. As the Orbach energy was generally higher for mutants S158A and Y160W, compared to wild-type protein (WT), it is suggested that H bonds removal influences the geometry leading to increased strength of antiferromagnetic coupling between two Fe ions of the cluster. While θ_D was similar for all variants (~107 K), the efficiency of Raman process generally depends on the spin-orbit coupling that is lower for S158A and Y160W mutants, when compared to WT. However, in several cases C_{Ram} did not correlate with spin-orbit coupling but was also influenced by other factors – possibly the modification of protein rigidity and therefore the vibrational modes around the Fe-S cluster that change upon the movement of the iron-sulphur head domain.

Introduction

Iron-sulphur proteins are common elements of many bioenergetic systems in which they play the role of electron carriers or constitute catalytic sites of enzymes involved in energy conversion [1]. The active sites of these proteins bind a compact inorganic cluster that usually contains two, three or four iron ions bridged by sulphur ions [2,3]. These clusters are chelated by proteins through either cysteine or, in the case of Rieske clusters, by cysteine and histidine side chains. A characteristic feature of the iron-sulphur clusters is the presence of strong antiferromagnetic coupling between high-spin iron ions that, depending on the redox state, leads to formation of diamagnetic (S=0) or paramagnetic state ($S=^1/_2$) in the centre with average *g*-tensor values lower than $g_e = 2.0023$ [4,5]. Electron paramagnetic resonance spectroscopy (EPR) is widely recognised as the main experimental tool to investigate the properties of paramagnetic iron-sulphur proteins [2,6].

The family of 2-iron-2-sulphur proteins is divided into two classes according to the average value of ***g*-tensor** principal components (g_{av}): ferredoxins with g_{av} ~1.96, and Rieske clusters with g_{av} ~1.91 [7]. The EPR spectra of clusters reveal a clear rhombic or close to axial symmetry.

Variations in *g* values observed for the Rieske clusters have been explained on the basis of a ligand-field model of antiferromagnetically coupled iron ions [8]. Modifications of *g* values are particularly associated with subtle changes in the ligand field around the Fe^{2+} ion which is coordinated by histidines. Additionally, the microheterogeneity of the protein environment around the cluster is a source of spread in the ligand field which is manifested as a *g*-strain effect in the EPR spectra of the clusters in frozen glassy solutions. A statistical theory for the *g*-strain tensor has been developed to describe asymmetry in the line shapes of the iron-sulphur cluster spectra linking the g-strain with rigidity of the protein core that binds the cluster [9,10].

The spin-lattice relaxation rate (T_1^{-1}) quantitatively describes how fast the energy absorbed by the spin is transferred to the phonons' bath and its value depends on the coupling strength of the relaxing paramagnet to the surrounding environment as well as on the vibrational modes of the

lattice. Commonly, the vibrational characteristics of the glassy frozen protein solution, constituting the "lattice" is described by the Debye model [11]. Temperature dependence of T_1^{-1} of proteins containing the [2Fe-2S] cluster has revealed existence of direct (one-phonon), second-order Raman and Orbach relaxation processes [12–14]. The second-order Raman process is recognised as a ubiquitous relaxation mechanism for all paramagnetic centres and its efficiency depends on several factors including the extent of spin-orbit coupling and rigidity of the protein that influences the vibrational modes of a paramagnetic centre [15,16]. In general, the larger the spin-orbit coupling (reflected as a deviation of the g-value from g_e) and the less rigid the structure, the higher the efficiency of the Raman process [17]. The Orbach mechanism requires the existence of a low-lying excited state which, in the case of iron-sulphur clusters, originates from antiferromagnetic coupling between high-spin iron ions [12,18].

The relaxation rates of iron-sulphur clusters have so far mainly been measured mainly for small proteins such as ferredoxins. In these cases, assigning changes in parameters of relaxation to specific structural details of proteins has generally been complicated by the fact that comparison involves different proteins coming from different organisms. In this study, we analysed T_1^{-1} of a reduced Rieske cluster $[2Fe\text{-}2S]^{2+}$ (Fe-S) of a large membrane protein complex - cytochrome bc_1 (Fig. 1 A) [19–21].

[Please, place FIGURE 1 here]

This protein provides a convenient model to compare T_1^{-1} of the same metalloprotein exposed to a variety of structural changes associated with modifications of both the local environment of the cluster and the global environment at the level of the whole protein. By term "local modifications" here we understand the changes in the structure of hydrogen bonds formed with the cluster or its ligands, while by "global modifications" we understand the changes in the position of the whole

iron-sulphur protein head domain (ISP-HD) in relation to other subunits of cytochrome bc_1.

The Fe-S cluster in cytochrome bc_1 is embedded in a water-exposed extrinsic domain (ISP-HD) that naturally undergoes a large-scale movement, inherent in the catalytic cycle of the enzyme. The movement allows the cluster to transfer electrons between the catalytic Q_o site in cytochrome *b* and heme c_1 on the cytochrome c_1 subunit [22–26]. At one extreme (the so-called "*b position*"), ISP-HD is in close contact with the Q_o site and the Rieske cluster interacts with the substrate bound at the site, while at the other extreme (the so-called "*c position*") ISP-HD is close to heme c_1 (Fig. 1 B). It has been shown in previous studies that the redox potential of the cluster varies significantly between these two positions – it is generally more than 100 mV higher at *b position,* compared to *c position* [25,27].

In isolated non-inhibited wild-type (WT) cytochrome bc_1, the ISP-HD is distributed between *b* and *c position* [26]. However, the average position of ISP-HD can be modified by introducing specific mutations that affect the motion and also by addition of specific inhibitors of cytochrome bc_1 [26,28,29]. Therefore, properties of the Fe-S cluster of cytochrome bc_1 can be studied under variety of conditions in which the position of the cluster can be controlled.

Here, we performed a detailed analysis of the spin-lattice relaxation rate of the Rieske cluster of cytochrome bc_1 isolated from *Rhodobacter capsulatus* under a variety of conditions to determine the basic parameters of the mechanisms that govern the relaxation between 5 K and 120 K particularly, Orbach energy and Debye temperature. We compared the effect of point mutations S158A and Y160W that remove the specific H bonds in the proximity of the cluster. We also investigated the effect on the efficiency of the Raman process of changes in the global distribution of positions of ISP-HD modified by using specific inhibitors and mutations.

Materials and methods

Bacterial strains, plasmids, and general molecular genetic techniques. Rb. capsulatus strains and *E.*

coli (HB101) were grown in MPYE (mineral-peptone-yeast-extract) and LB media, respectively, supplemented with appropriate antibiotics as needed [30]. Photosynthetic growth of *Rb. capsulatus* strains was tested on MPYE plates using anaerobic jars (GasPak System, BBL) at 30 °C under continuous light. *Rb. capsulatus* strains with mutated cytochrome bc_1 were generated as described previously [31], using the genetic system developed by Prof. F. Daldal (University of Pennsylvania, Philadelphia, USA). The templates containing the desired mutations were obtained using the QuickChange ® protocol (Stratagene). Changes to the *petA* gene (coding for the ISP subunit) resulting in the mutations S158A or Y160W were introduced by PCR using DNA as a template: pPET1 (for construction of single mutants S158A or Y160W), pPET1 containing mutations for +1Ala or +2Ala insertions [23] (for construction of double mutant S158A+1Ala or S158A+2Ala, respectively). The 1 kb *BstX*I/*Xma*I fragments containing desired mutations (and no other mutations, as confirmed by DNA sequence analysis) were exchanged with their wild-type counterparts in pMTS1 to construct mutated variants of pMTS1. These were used as expression vectors in *Rb. capsulatus* cells. They were introduced into the MT-RBC1 strain (*pet*ABC-operon deletion background) via triparental crosses as described in [31]. In each case, the presence of engineered mutations was confirmed by sequencing the plasmid DNA isolated from the mutated *Rb. capsulatus* strains.

Biochemical procedures. Cytochrome bc_1 complex was isolated from purple bacteria *Rb. capsulatus* grown under semiaerobic conditions, according to the procedure described previously in [32]. The concentration of isolated protein (per cytochrome c_1 content) was determined spectrophotometrically using ascorbate-reduced minus ferricyanide-oxidised differential spectra and extinction coefficient $\varepsilon_{552\text{-}542nm}$ = 20 mM^{-1}. All forms of cytochrome bc_1 were dialysed against buffer containing 50 mM bicine pH 8, 100 mM KCl, 1 mM EDTA, 20% (v/v) glicerol and 0.01% dodecyl maltoside. Inhibitors: tridecyl stigmatellin (*tds*), myxothiazol (*myx*), famoxadone (*fam*),

atovaquone (*ato*) and antimycin (*ant*) were added from DMSO stock solution to obtain a molar excess over the protein. The inhibitors were purchased from Sigma-Aldrich, except for *tds*, which was a generous gift from Dr N. Fisher. All forms of cytochrome bc_1 bind inhibitors with similar affinity as inferred from enzymatic turnover assays and light-induced electron transfer measurements (data not shown).

The measurements of enzymatic activity of the different forms of cytochrome bc_1 were performed as described in [33] using 20 μM horse cytochrome *c*, 20 μM decylubihydroquinone and 10-100 nM of the enzyme.

Equilibrium redox titrations of the Fe-S cluster were performed on isolated protein at pH 8. To minimise pH shift upon freezing the bicine buffer was used [34]. The following redox mediators were applied: tetrachlorohydroquinone, diaminodurol, 1,2-naphtoquinone-4-sulfonate, phenazine methosulphate, phenazine ethosulphate, 1,2-naphtoquinone. Ambient redox potential was adjusted by addition of small aliquots of potasium ferricyanide or sodium dithionite solutions. For each point of ambient potential a small portion of the sample was anaerobically transferred to an EPR tube and frozen in liquid nitrogen. Spectra of titrated protein were subsequently measured by CW EPR at 20 K and redox potential was determined by fitting the Nernst equation to the data points (Fig. S1).

Prior to EPR measurements all samples of cytochrome bc_1, except those prepared for redox titration, were reduced with sodium dithionite to keep all the protein cofactors in reduced state. After reduction samples were frozen and stored in liquid nitrogen until used.

EPR measurements. EPR spectroscopy was performed on a Bruker Elexsys E580 spectrometer operating at X- and Q-band using similar equipment and settings as described previously in [26,35]. CW spectra were recorded at X-band at a temperature range between 20 – 120 K using non-saturating microwave power.

Inversion recovery measurements between 5 – 25 K. Pulse EPR experiments were carried

out in the Bruker Q-band resonator ER5107D2. Inversion recovery (IR) measurements were performed at 5 - 25 K using a pulse sequence: $\pi - t_d - {}^{\pi}/_{2} - t - \pi$ with constant t = 160 ns. The initial t_d = 160 ns was incremented to cover the whole recovery curve after the inverting π pulse. Such sequence setup yields overall dead time of IR measurement equal ~500 ns. Within the considered temperature range the relation: $T_1 >> T_2$ is valid, therefore transverse relaxation does not affect the measured IR curves [26]. The lengths of microwave pulses ${}^{\pi}/_{2}$ and π were set to 20 and 40 ns, respectively and the microwave pulse power was adjusted to obtain the maximum amplitude of the spin echo. Above 25 K the relaxation becomes very fast and most of the recovery takes place within the experimental dead time, therefore only residual slow-relaxing components of the recovery can be detected. Above 30 K the spin-echo signal becomes virtually undetectable.

The measured IR curves were non-exponential, indicating the distribution of relaxation rates or spectral diffusion. To evaluate possible effect of "spectral diffusion" on the recorded IR trace we performed measurements in which the first inverting π pulse was replaced with a saturating picket-fence of microwave pulses, or with a single saturating long-pulse. However, in all cases the of shape of recovery curves remained unchanged. The experimental IR curves were mathematically modelled with a stretched exponent function:

$$Y(t) = a \cdot \exp\left[-\left(\frac{t}{\tau}\right)^{\beta}\right] + y_0$$

where: τ and β represent the time constant of the process and stretching parameter, respectively.

The average spin-lattice relaxation rate was then calculated using the equation:

$$\frac{1}{T_1} = \left[\Gamma\left(\beta^{-1}\right)\frac{\tau}{\beta}\right]^{-1}$$

where Γ is the gamma function [36].

For *tds*-treated WT, S158A and Y160W and for non-inhibited S158A, WT, Y160W, and +2Ala, S158A+1Ala IR curves were measured at g_z, g_y and g_x transitions. In all cases the obtained

T_1 values depended on their position on the Fe-S spectrum, proving the anisotropic character of the relaxation. In the presence of *tds*, the spin-lattice relaxation rate increased in the order: $(1/T_1)g_x < (1/T_1)g_y < (1/T_1)g_z$ while for non-inhibited enzymes a different relationship occurred: $(1/T_1)g_y < (1/T_1)g_x < (1/T_1)g_z$. The origin of these changes in the relaxation anisotropy upon addition of *tds* is not known but probably it could be associated with formation of the hydrogen bond between the inhibitor and the cluster liganding histidine 156. In further analyses only T_1 determined at g_y transition was considered.

Analysis of CW EPR spectra and determination of T_1 for temperatures above 80 K

At temperatures higher than 40 K, T_1 shortens and drives transverse relaxation ($T_2 = T_1$). As temperature increases, the homogeneous broadening of the individual resonance lines rises with T_1^{-1}, affecting the width of the inhomogeneous lines, observed in the CW EPR powder spectrum. Estimation of ***g*** and ***g*-strain** tensors, as well as the temperature-dependent Lorentzian broadening for a particular variant of cytochrome bc_1 results from the fitting of the simulated EPR spectrum to experimentally measured traces.

A model of "powder" EPR spectrum simulation, adequate for frozen solutions of metalloproteins (with $S=^1/_2$) was developed by Hagen [37]. In our simulations we implemented the basic foundations of Hagen's algorithm: the ***g* - strain** tensor was defined in the *g*-values space, and its components (up to six) determined an orientation-dependent Gaussian linewidth $\gamma_G(\theta,\varphi)$ of the resonance transition at $g_{eff} = g(\theta,\varphi)$. Additionally, tensor ***L*** (expressed in term of *g*-values space) was incorporated into the model to account for the presence of anisotropic homogeneous broadening. The principal values of the ***L*** tensor were used to calculate the effective value of the Lorentzian linewidth $\gamma_L(\theta,\varphi)$ by an expression analogical to that used for the Gaussian linewidth $\gamma_G(\theta,\varphi)$. The subsequent lineshape for a given resonance line resulted from convolution of the Gaussian and lorentzian broadening mechanisms which for practical reasons was approximated by the pseudo-

Voigt profile [38,39]. The simulated EPR spectrum was created as a superposition of all calculated signals originating from particular centres that were randomly oriented with respect to the applied magnetic field. This was performed as an orientation-weighted sum over a sphere represented by a SOPHE grid [40,41], which typically consisted of 1000 orientations. Each spectrum was transformed from the *g*-values domain to the magnetic field domain using proper renormalization formulas. All numerical simulations of the EPR spectra were implemented in a Matlab environment, using original written procedures (available upon request). The values of ***g***, ***g*-strain** and ***L*** were determined for all examined cytochrome bc_1 samples as the "best fit" parameters. Initially, the simulated spectra were fitted using the Simplex method and then further optimised using the Levenberg-Marquardt algorithm (LMA). For temperatures where $T_2 = T_1$, based on the fitted values of ***L*** tensor, the spin-lattice relaxation rates for each line $i = x, y, z$ were calculated using the formula:

$$\frac{1}{T_{1i}} = 2\pi v \frac{L_i}{g_i}$$

where v is the microwave frequency, L_i denotes the principal value of the ***L*** tensor (full width at half maximum (FWHM) of the Lorentzian line in the *g*-value domain) and g_i is the principal value of the *g*-tensor.

In case of multicomponent spectra the average relaxation rate was calculated as the weighted mean value of relaxation rates obtained from ***L*** tensor for each spectral component.

Analysis of temperature dependence of relaxation rate of Rieske cluster.

Spin-lattice relaxation rates of different forms of cytochrome bc_1, determined for the whole temperature range 5–120 K, were fitted using LMA as the sum of three mechanisms: direct, Raman and Orbach:

$$\frac{1}{T_1} = C_{dir}T + C_{Ram}\left(\frac{T}{\theta_D}\right)^9 J_8\left(\frac{\theta_D}{T}\right) + C_{Orb}\cdot E_{Orb}^3\left[\exp\left(E_{Orb}T^{-1}\right)-1\right]^{-1}$$

In this equation C_{dir}, C_{Ram}, C_{Orb}, θ_D and E_{Orb} are the efficiencies of direct, Raman and Orbach processes, respectively. θ_D and E_{Orb} denote Debye temperature and Orbach energy, respectively. The transport integral J_8 was substituted with an analytical approximation, as described in [42], which allowed us to fit θ_D as an independent parameter. The uncertainty levels of the determined "best-fit" parameters were obtained from square roots of diagonal elements of the covariance matrix, calculated by LMA. To compare C_{Ram} for different samples we performed additional fitting of the data obtained in a temperature range between 10 K and 25 K with the θ_D value fixed at 107 K, which is the average Debye temperature determined for all samples.

To compare spectral anisotropy between different samples we introduced a phenomenological parameter *A,* that provides the averaged (over the whole EPR spectrum) measure of spin-orbit coupling. *A* is defined as:

$$A = \sqrt{\sum_{i}^{n}\left[(g_e - g_i)^2 \cdot f(g_i) \cdot \Delta g\right]}$$

where *i* is a consecutive point of a simulated spectrum in the *g*-value domain, *n* is the total number of points of the digitised spectrum, $f(g_i)$ is the amplitude of the absorption spectrum at g_i position, g_e is the *g*-value of the free electron, g_i is the consecutive *g*-value and Δg is the resolution. The value of "*A*", calculated on the basis of the EPR spectrum for a disordered sample, is sensitive not only to the deviation of the adequate **g**- tensor from g_e, but also to the sample-specific distribution $f(g_i)$. Thus the proposed formula more reliably reflects the effective strength of spin-orbit coupling and can differentiate those samples with similar g-tensors but different EPR spectrum shapes.

Results and discussion

Effect of mutations and inhibitors on the position of ISP-HD and redox properties of Fe-S cluster.

We analysed the properties of ISP in the presence of various mutations and/or inhibitors of quinone catalytic sites. All these factors introduced structural changes in the local environment of the Fe-S and some of them also influenced the average distribution of ISP-HD positions. The

mutations affecting the motion included insertions of one or two Ala residues in position 46 [23,24] (+1ALA or +2ALA) leading to a shift of various degrees of the population of ISP-HD towards the cytochrome *b* subunit (to the *b position*) (Fig. 1 B). In +1ALA, the ISP-HD is arrested at the *b position* for at least several milliseconds which leads to only a slight decrease in the enzymatic activity of cytochrome bc_1 [27,29,43,44]. In +2ALA the ISP-HD is arrested at this position for hundreds of milliseconds, which relegates the electron transfer between Q_o and heme c_1 at the time scale of seconds severely inhibiting the enzymatic activity. The mutations in the local environment of the Fe-S cluster included replacement of either S158 to Ala or Y160 to Trp (Fig. 1 C). S158A removes the hydrogen bond between the -OH group of serine and the S1 sulphur of the cluster, whereas changing Y160 to Trp not only removes the hydrogen bond between the -OH group of tyrosine and the sulphur atom of the cluster liganding C133 but also slightly shifts the positions of amino acid side chains around the cluster shell to accommodate a relatively large tryptophane residue [45–48]. S158A was tested alone (single mutant S158A) or in combination with +1Ala and +2Ala (double mutants S158A+1Ala and S158A+2Ala, respectively).

Table 1. Equilibrium redox midpoint potentials of the Fe-S cluster in WT and mutants of cytochrome bc_1, the ability of the enzyme to support photosynthetic growth of *Rhodobacter capsulatus* cells and enzymatic activity of the enzyme.

Form	$\Delta E_{m,pH\,8}$ [mV]	Photosynthetic growth	Turnover rate of cytochrome *c* reduction [s^{-1}] ± st. error
WT	0	+++	140 ± 5
+1ALA	+13	+++	144 ± 7
+2ALA	+89	-	4.2 ± 0.2
S158A	-133	+	18.1 ± 0.6

Y160W	-103	++	11.9 ± 0.2

As shown in Table 1, S158A and Y160W decreased E_m by ~133 and ~100 mV, respectively. This is reflected in the changed viability of the mutant cells to grow under photosynthetic conditions [footnote] and lowered enzymatic activity. The changes in the E_m of S158A and Y160W are associated with the removal of hydrogen bonds in the vicinity of the cluster as anticipated from inspection of the crystal structure of analogue mutants in *Rhodobacter sphaeroides* and biochemical studies of mutated ISP from other organisms [47–49].

Table 1 shows that +1Ala and +2Ala also influence E_m, as reported earlier [27]. When ISP-HD is in *b position*, the redox potential of Fe-S is higher compared to the potential of Fe-S in other positions [27]: thus, in +2Ala, in which almost the entire population is in *b position*, the redox potential is elevated by ~ 90 mV while in +1Ala, in which the population at *b position* is larger than in WT but less than is the case for +2Ala, the potential is elevated by ~ 20 mV. The increase in the redox potential upon shifting the ISP-HD to *b position* (+1Ala or +2Ala) appears to be independent from the effect of hydrogen bonding as it is also observed for mutants with shifted ISP-HD and lacking specific H bonds (see example S158A vs S158A+1Ala in Fig. S1). The origin of the change in redox potential of Fe-S related to the change in position of the ISP- HD is still not clear [25,50], but it is likely related to distortions of the active site upon binding ISP-HD to the Q_o site that modifies the ionisation potential of the cluster [4,51].

Inhibitors of the Q_o catalytic site included *tds*, *ato*, *fam* and *myx* [52,53]. The first three inhibitors (*tds*, *ato*, and *fam*) fix the ISP-HD domain at the *b position*, which can occur with (*tds* and *ato*) or without (*fam*) formation of a hydrogen bond between the inhibitor and cluster-liganding H156 residue. Myxothiazol has the opposite effect; it shifts the domains out of the *b position* [54].

Inversion recovery rates of the Rieske cluster at 12 K

Fig. 2 A shows inversion recovery curves measured at 12 K at the g_y transition of the Fe-S cluster for samples in which the distribution of positions of ISP-HD was modified by +1Ala mutation or by using inhibitors *tds* or *myx*. The recovery rate increases in the order WT+*tds* < +1Ala < WT < WT+*myx* (11.3×10^3, 12.1×10^3, 15.2×10^3, 18.3×10^3 s^{-1}, at 12 K respectively) and appears to correlate with the shift of ISP-HD out of the *b position*: the domains that are closer to the *b position* exhibit slower recovery rates.

[Please place FIGURE 2 here]

The effect of point mutations S158A and Y160W on T_1 was initially tested in the presence of *tds* to eliminate possible influence from changes in the distribution of ISP-HD positions on T_1. The relaxation rate for these samples increased in the order of S158A+*tds* < Y160W+*tds* < WT+*tds* (4.5×10^3, 6.1×10^3 and 11.3×10^3 s^{-1} at 12 K respectively) (Fig. 2 B). This effect must result from modifications in the local protein structure near the Fe-S cluster binding site, in particular the lack of specific hydrogen bonds in the mutants.

Analysis of CW EPR spectra of the Fe-S cluster at low temperature.

The modification of the cytochrome bc_1 structure caused by mutations and/or inhibitors affected the features of CW EPR spectra of the Rieske cluster in particular samples; however, the general rhombic shape was preserved in all cases (see examples in Fig. 3).

[Please place FIGURE 3 here]

Simulation of CW EPR spectra at 25 K allowed us to estimate the principal ***g*** tensor and *g*-strain values that define the inhomogeneous line broadening and the number of components in the

particular CW spectrum (see Table S1 in Supporting Information). Introducing off-diagonal elements of the ***g*-strain** tensors did not improve the fits thus in all cases only principal *g*-strain values were considered.

The use of one spectral component was only sufficient to simulate spectra only for samples in which ISP-HD was fixed at *b position* due to the presence of mutation (+2Ala, S158A+2Ala) or inhibitor *tds* (WT+*tds*, S158A+*tds*, Y160W+*tds*). This observation suggests that *tds* or +2Ala mutants arrest ISP-HD at *b position* in such way that the population of the Fe-S clusters is uniform and single-component. Other inhibitors that also restrict the motion of ISP-HD (*ato*, *fam*) required the introduction of two components, with clearly different **g**-tensors, to reproduce the experimental spectra. In the presence of *ato*, addition of ~18% of the second component was needed, while in the presence of *fam*, the two components contributed almost equally. The difference in the number of components between *tds* and *ato* or *fam* can be explained by the fact that *ato* and *fam* are not as strong inhibitors as stigmatellin and that the hydrogen bond between inhibitor and ISP-HD is weaker (*ato*) [55–57] or not formed at all (*fam*) [52,58,59]. The remaining spectra also required more than one component to obtain good fits but generally two components were sufficient to reproduce all experimental spectra. Fig. S2 shows the inadequacy of selected single-component fits.

Point mutations S158A and Y160W led to an increase in ***g*** values and decrease in both average spectral anisotropy and *g*-strain values of the Fe-S cluster, when compared to WT. This effect is associated with the changes in an electronic configuration due to modifications of hydrogen bonds around the Fe-S cluster. The addition of *myx* to the samples led to only small changes in *g* values and *g* strain. Representative results of spectral simulations for WT, S158A and Y160W, in combination with *tds* and *myx* are shown in Fig. 3.

Spin-lattice relaxation rate obtained from simulation of CW spectra at higher temperature.

For simulations of spectra registered in the temperature range of 80 - 120 K only

homogeneous broadening was considered to change upon increases in the temperature. The other parameters (e.g. *g* values, *g* strain, number of components etc.) were fixed at values established from simulations of respective spectra at 25 K. This assumption was justified by the fact that temperatures below 120 K are still low enough to keep the protein structure unchanged in comparison to the structures at 25 K.

In several cases, the fitting of the CW spectra using a model with isotropic Lorentzian broadening led to an unacceptably poor fits (see examples for WT and WT+*myx* shown in Fig 4). Given that, and also taking into account the anisotropy of IR rates, we concluded that the broadening of the lines must be described by anisotropic Lorentzian linewidth. Indeed, the anisotropic model of Lorentzian broadening significantly improved the fits (Fig 4). Clearly, at higher temperatures the relaxation follows the anisotropic trend observed at low temperatures and this anisotropy is even more pronounced.

[Please place FIGURE 4 here]

Mechanisms of spin-lattice relaxation of the Fe-S cluster.

A physical explanation of the spin-lattice relaxation process must refer to the electronic states of the exchange-coupled diiron cluster and the vibrational properties of the lattice. When modifications of the structure surrounding the paramagnetic centre affect the protein vibrational modes, the measured T_1 values will differ between variants of cytochrome bc_1. Within the investigated temperature range (5 – 120 K) we consider the existence of three relaxation mechanisms: direct, Orbach, and second-order Raman processes, as inferred from the characteristic temperature dependence of $1/T_1$ (see Fig. S3 for linear representation of relaxation rate typical for Raman or Orbach processes).

In Fig. 5, two representative curves of the relaxation rate as a function of temperature

between 5-120 K are shown. In the range 10 – 25 K, $1/T_1$ increases with approximately a sixth power of temperature, indicating domination of the second-order Raman process. Above 80 K this dependence is exponential, suggesting the contribution from the Orbach process, which starts to dominate upon an increase in temperature. At the lowest temperatures (below 10 K), a contribution from the direct process can be recognised from the observation that IR curves are frequency-dependent (the relaxation rates measured at Q band are higher than those measured at X band). This frequency-dependence becomes undetectable upon a rise in the temperature as other mechanisms prevail (data not shown). Fig. 5 also shows representative fits of the sum of these three mechanisms to the experimental data points yielding parameters shown in Table 2. For all forms of cytochrome bc_1 investigated here, Debye temperature falls within the range 100 – 120 K (with an average value of 107 K), which is in agreement with values reported for frozen glassy solutions of proteins [15]. The Orbach energy falls within the range ~ 350–550 K with the average value ~ 450 K (~ 300 cm^{-1}), which also is in the same order as previously reported values for ferredoxins [14,60].

[Please place FIGURE 5 here]

Comparison of WT with S158A and Y160W indicates that the Orbach energy increases in those mutants (353 K for WT vs 447 and 554 K in S158A and Y160W, respectively), suggesting an increased antiferromagnetic coupling between Fe ions in the cluster. This effect is likely to be related to subtle changes in the geometry of the Fe-S cluster particularly in terms of the Fe – S distance and/or Fe – S – Fe angle[61]. Inhibitors and mutations affecting motion of ISP-HD also influence the Orbach energy, but at this point it is difficult to find a clear tendency for these changes (Table 2).

Efficiency of Raman relaxation in different forms of cytochrome bc_1

Parameters describing the efficiency of Raman relaxation and Debye temperature are correlated[62]. This means that changes in C_{Ram} can be compensated by changes in θ_D. Therefore, to compare C_{Ram} for different samples, θ_D was kept constant at 107 K and only Raman efficiency was fitted yielding C'_{Ram} values.

The point mutation around the Fe-S cluster (S158A or Y160W) has a dominant effect on the relaxation rates thus, the influence of other factors differentiating the samples was further examined within 3 groups: A – encompassing WT variants with the presence or absence of different inhibitors and +1Ala, +2Ala insertions; B – S158A variants with or without inhibitors or +1Ala, +2Ala insertions; and C – Y160W variants with or without inhibitors. The values of C'_{Ram} were compared within each of these groups.

Such analysis revealed the following regularities. When ISP-HD is fixed at *b position* due to the presence of *tds*, *ato*, *fam* or mutation +2Ala, the efficiency of Raman process decreases. On the other hand, the inhibitors that shift the ISP-HD distribution out of the *b position* (*myx*, and *myx*+*ant*) cause the C'_{Ram} to increase in comparison to non-inhibited enzyme. These results suggest that the relaxation efficiency of Raman processes for the Fe-S cluster in cytochrome bc_1 generally correlates with an increase in the average distance of ISP-HD from the *b position*.

The efficiency of Raman relaxation generally rises with an increase in spin-orbit coupling, which is proportional to the difference between *g*-values and $g_e = 2.0023$. It is also known that for paramagnetic centres with comparable spin-orbit coupling the efficiency is smaller for structures that are more rigid. Therefore, to estimate possible contribution from spin-orbit coupling and protein rigidity, we analysed the dependence of C'_{Ram} on the average spectral anisotropy A (Fig. 6).

[Please place FIGURE 6 here]

The experimental data, depicted in Fig. 6, confirmed the expected general tendency for an increase

in C'_{Ram} with growing spin-orbit coupling. However, close inspection of the data in Fig. 6 reveals several cases for which an increase in spectral anisotropy does not lead to an increase in C'_{Ram} (for example C'_{Ram} in S158A+1Ala = S158A = Y160W+*tds*, S158A+2Ala = S158A+*tds* or +2Ala = WT+*fam* = WT+*ato*) or an increase in C'_{Ram} is not associated only with a change in spectral anisotropy (for example, C'_{Ram} in S158A+*tds* < S158A < S158A+*myx*, WT < WT+*myx* < WT+*ant*+*myx*). There is even a case for which C'_{Ram} decreases while spectral anisotropy increases (compare C'_{Ram} in a series +1Ala > Y160W+*myx* > WT+*tds* > Y160W > WT+*ato*).

Considering the black points in Fig. 6 (all describing different forms of S158A), one can predict that of the two forms of Fe-S clusters with ISP-HD arrested at *b position* (S158A+2Ala and S158A+*tds*) the one, with inhibitor *tds*, is probably more rigid. On the other hand, the Fe-S core becomes less rigid as the population of clusters is shifted out of the *b position* (C'_{Ram} in S158A+*tds* < S158A < S158A+*myx*). A similar trend can be observed when the ISP-HD in WT is shifted out of *b position* (compare C'_{Ram} for WT < WT+*myx* < WT+*ant*+*myx* - blue points in Fig. 6). This suggests that the rigidity of the Fe-S cluster changes depending on its position, and it is generally larger when Fe-S is in contact with the catalytic Q_o site (*b position*). Additionally, in the *b position* the rigidity appears to be modified by the presence and the type of inhibitor that occupies the site (compare for example: +2Ala, WT+*fam* and WT+*ato*). This is probably related to the capability of an inhibitor to create a hydrogen bond with cluster-liganding H156.

Interestingly, Fig. 6 shows examples of C'_{Ram} values that are negatively correlated with spectral anisotropy. This is best seen for the series +1Ala, Y160W+*myx*, WT+*tds*, Y160W and WT+*ato*. To explain this result, we propose that the effect of an increase in spin-orbit coupling is compensated or even dominated by the progressive increase in the rigidity of the protein.

Effect of changes in hydrogen bonding on the Raman relaxation of the Fe-S cluster

The series of samples studied here allowed us to evaluate the effect of two types of hydrogen bonds

on the efficiency of Raman relaxation. The first type involved intramolecular H bond located within the core of the Fe-S cluster (between the OH group of S158 and S1 of the cluster or the OH group of Y160 with the S atom of cluster-liganding C133) while the second type involved the intermolecular bond between the inhibitor occupying the catalytic Q_o site within the cytochrome *b* subunit and cluster-liganding H156 on ISP-HD.

Removing the intramolecular H bond in S158A or Y160W leads to a decrease in C'_{Ram} which may result from changes in vibrational modes and/or spin-orbit coupling. While at this stage separating contributions from these two factors is difficult, one can expect that, if the effect of changes in vibrational modes is significant, then the intramolecular H bond provides an additional channel to transfer vibrations from the surroundings to the paramagnetic centre (Fe-S). On the other hand, an addition of the intermolecular H bond in the presence of the inhibitor may lead to an increase in the rigidity of the Fe-S binding core, probably due to the introduction of additional constraint to the motion when two subunits of cytochrome bc_1 (cytochrome *b* and ISP) are in close contact and are additionally stabilised by interactions with the bound inhibitor. However this interpretation should be treated with caution, as at this level we have no data on the vibrational modes of lattice for the different variants of the cytochrome bc_1.

Concluding remarks

In this study we examined changes in T_1 of the Rieske cluster in cytochrome bc_1 induced by several structural factors. Removal of H bonds in S158A or Y160W significantly increases T_1 of the Fe-S cluster. A somewhat weaker but similar effect was observed when the distribution of the positions of ISP-HD (induced by mutations +1Ala, +2Ala or inhibitors) was shifted to the *b position* (to catalytic Q_o site) and this effect was independent of changes in H bonding. Therefore, the measurement of T_1 offers a way to monitor the general position of ISP-HD with a reduced Fe-S cluster, irrespective of the redox state of the remaining cofactors of cytochrome bc_1. This is

provided that mutants with the same intramolecular H bonding pattern are compared. This means that this is complementary to the previously described method of monitoring the ISP-HD distribution that was based on the measurement of the phase-relaxation-enhancement of the Fe-S cluster induced by the relaxation of heme b_L. The latter method obligatorily required the presence of oxidised heme b_L that can interact with the Rieske cluster via dipolar interaction [26].

The spin-lattice relaxation rate of the Fe-S cluster revealed the existence of significant anisotropy, which becomes more pronounced as temperature increases. Above 80 K, it is so large that simulation of the CW EPR spectra of the cluster must include the anisotropic ***L*** tensor which defines different Lorentzian broadening for the g_z, g_y, and g_x transitions.

The temperature dependence of the relaxation rates can be explained by assuming the presence of direct (below 5 K), Raman (dominating between ~10 – 25 K) and Orbach (dominating above ~ 80 K) processes. The presence of these mechanisms in the Rieske cluster of cytochrome bc_1 is in agreement with mechanisms described for spin-lattice relaxation of other iron-sulphur clusters in small proteins such as ferredoxins [18,63].

The average Orbach energy reflecting antiferromagnetic coupling of the Rieske cluster in cytochrome bc_1 was approximately 450 K (~300 cm^{-1}) which is similar to other iron-sulphur proteins. We found that eliminating specific H bonds between the protein and sulphur atom of the cluster or sulphur atom of the cluster-liganding C133 leads to general increase in the Orbach energy and may suggest that distances or angles between cluster atoms undergo modifications resulting in stronger spin-spin exchange coupling between Fe^{3+} and Fe^{2+} ions of the Fe-S cluster.

The efficiency of the Raman process (C_{Ram}) generally increased exponentially with an increase in spectral anisotropy A (related to the spin-orbit coupling). Nevertheless, for some samples characterised by rather large spectral anisotropy, the expected increase of C'_{Ram} was not observed. This lack of correlation can be interpreted as a reflection of changes in the rigidity of the protein that leads to modification of vibrational modes of the Fe-S cluster, that overlays with the

effects of changes in spin-orbit coupling. This suggests that upon formation or breaking of inter- or intramolecular hydrogen bonds and/or modification of interactions of the ISP-HD with other subunits of cytochrome bc_1 the flexibility of surroundings for the vibrational motions of the Fe–S cluster changes. It can be speculated that these changes contribute to the overall setting of the electrochemical properties of the cluster and may influence electron transfer between Fe–S and its redox partners during the reactions catalysed by cytochrome bc_1 [61].

Table 2. Parameters of spin-lattice relaxation for different forms of Rieske cluster.

Group	Sample	C_{Dir} [s^{-1} K^{-1}]	C_{Ram} [$s^{-1}K^{-9}$] × 10^{-10}	θ_D [K]	C_{orb} [$s^{-1}K^{-3}$]	Δ_{orb} [K]
A	WT	24.0 ± 3.2	1.59 ± 0.16	108 ± 4	966 ± 130	353 ± 29
	WT + *tds*	24.8 ± 2.9	1,24 ± 0.11	103 ± 3	612 ± 59	398 ± 25
	WT + *myx*	33.9 ± 5.7	1.86 ± 0.22	109 ± 5	1052 ± 225	406 ± 46
	WT + *ato*	40.3 ± 9.4	0.91 ± 0.17	111 ± 6	nd	nd
	WT + *fam*	23.0 ± 2.3	0.98 ± 0.07	104 ± 3	nd	nd
	WT + *ant+myx*	22.7 ± 6.8	1.96 ± 0.24	110 ± 5	nd	nd
	+1ALA	27.1 ± 2.9	1.39 ± 0.12	102 ± 3	907 ± 144	505 ± 28
	+2ALA	31.8 ± 4.0	0.913 ± 0.090	108 ± 3	444 ± 43	410 ± 25
B	S158A	14.3 ± 2.4	0.441 ± 0.066	118 ± 5	234 ± 49	447 ± 48
	S158A + *tds*	14.8 ± 1.2	0.411 ± 0.031	109 ± 3	364 ± 24	465 ± 16
	S158A + *myx*	16.0 ± 1.8	0.77 ± 0.08	101 ± 3	nd	nd
	S158A+1ALA	17.1 ± 2.0	0.71 ± 0.06	99 ± 3	345 ± 26	523 ± 16

	S158A+2ALA	21.5 ± 2.3	0.455 ± 0.046	108 ± 3	222 ± 22	470 ± 30
C	Y160W	20.6 ± 3.3	1.09 ± 0.13	108 ± 4	4290 ± 1077	554 ± 64
	Y160W + *tds*	14.4 ± 1.2	0.599 ± 0.041	107 ± 3	469 ± 34	425 ± 18
	Y160W + *myx*	23.1 ± 4	1.15 ± 0.13	104 ± 4	nd	nd

Associated content

Footnote

Rb. capsulatus obligatorily requires functional cytochrome bc_1 to support photosynthetic growth of the bacteria in the absence of oxygen; therefore viability of growth under these conditions reflects the general activity of the enzyme.

Acknowledgement

This study was supported by The Wellcome Trust International Senior Research Fellowship (to A.O.) and by the Polish Ministry of Science and Higher Education grant Iuventus Plus (to M.S.).

We would like to thank Dr Monika Czapla for preparation of mutants of cytochrome bc_1.

Abbreviations

EPR, electron paramagnetic resonance; Fe-S, iron-sulphur; ISP, iron-sulphur protein subunit; ISP-HD, movable head domain of iron-sulphur protein subunit; *tds*, tridecyl-stigmatellin; *ato*, atovaquone; *fam*, famoxadone; *myx*, myxothiazol; *ant*, antimycin, E_m, redox midpoint potential; IR, inversion recovery, CW, continuous wave; θ_D, Debye temperature, LMA, Levenberg-Marquardt algorithm.

Supporting information

Fig. S1: Results of equilibrium redox titration of Fe-S cluster for different forms of cytochrome bc_1;

Fig. S2: Selected results of simulations of X-band CW EPR spectra of the Rieske cluster recorded at 25 K with a single-component model; Fig. S3: Temperature dependence of spin-lattice relaxation rate ($1/T_1$) of the Rieske cluster for *tds*-inhibited WT in linearized form for Raman and Orbach processes; Table S1: Values of **g** and **g-tensor** components determined from fitting the two-component model to X-band CW EPR spectra (25 K) for different forms of cytochrome bc_1.

Figure legends

Fig. 1. Crystal structure of cytochrome bc_1 and structural details of ISP protein. (A) Ribbon model of native cytochrome bc_1 dimer from *Rhodobacter capsulatus* (pdb id 1ZRT [20]) containing three catalytic subunits: cytochrome *b* – green, cytochrome c_1 – red, and ISP – magenta). Grey area denotes the location of the membrane bilayer. (B) Model of one monomer of cytochrome bc_1 with overlaid different positions of ISP-HD. The Fe–S cluster is shown in b-, c- and intermediate positions as yellow-red spheres. Sticks represent hemes c_1, b_L and inhibitor stigmatellin. The positions of the ISP-HD were taken from structures in pdb database: 1BCC[22], 1BE3[64], 1BGY[64] and 1ZRT[20]. (C) The local environment of Fe-S cluster at *b position* in the presence of stigmatellin that forms hydrogen bond with cluster-liganding H156. Yellow dashed lines indicate the H–bonds and magenta dotted lines represent bonds between cluster ligands and iron ions of the cluster. Green and magenta ribbons represent cytochrome *b* and ISP subunits.

Fig. 2. Semi-log plot of inversion recovery curves measured at g_y transition of Fe-S cluster at 12 K. Comparison of recovery curves for cytochrome bc_1 with different average position of ISP-HD in the absence of point mutations (A) and for S158A or Y160W mutants with ISP-HD arrested at *b position* by treatment with *tds* (B).

Fig. 3. Simulation of X-band CW EPR spectra measured at 25 K of Fe-S cluster for WT, S158A and

Y160W mutants. Spectra from left to right correspond to forms in which average distance of Fe-S cluster from *b position* increases. Solid grey and dashed black lines show experimental and simulated spectra, respectively.

Fig. 4. CW EPR spectra of the Fe-S cluster measured at 100 K for non-inhibited WT cytochrome bc_1, treated with tridecyl-stigmatellin (*tds*) and myxothiazol (*myx*). Solid grey and dashed black lines show experimental and simulated spectra, respectively. Left and right columns show the results of fitting the same experimental data with model assuming isotropic and anisotropic Lorentzian broadening of the lines, respectively.

Fig. 5. Log-log plot of temperature dependence of spin-lattice relaxation rate of the Fe-S cluster obtained for *tds*-treated WT and S158A (open and closed symbol, respectively). Solid line shows the fit of direct, Raman and Orbach process to experimental data. Dashed lines show the contribution from these three processes to the relaxation of Fe-S in mutant S158A in the presence of *tds*.

Fig. 6. Efficiency of Raman process (C'_{Ram}) plotted as a function of spectral anisotropy determined for WT (blue) and mutants +1Ala and +2Ala (green), Y160W (red) and S158A (black) in combination with different inhibitors that influence the average position of ISP-HD. Black dotted line represents the exponential growth fit to guide eye.

References

(1) Beinert, H. Iron-Sulfur Proteins: Ancient Structures, Still Full of Surprises. *J. Biol. Inorg. Chem.* **2000**, *5* (1), 2–15.

(2) Cammack, R.; MacMillan, F. Electron Magnetic Resonance of Iron-Sulfur Proteins in Electron-Transfer Chains: Resolving Complexity. In *Metals in Biology:applications of High-resolution EPR to Metalloenzymes, Biological Magnetic Resonance*; Hanso, G., Berliner, L., Eds.; 2010; Vol. 29, pp 11–44.

(3) Brzóska, K.; Męczyńska, S.; Kruszewski, M. Iron-Sulfur Cluster Proteins: Electron Transfer and beyond. *Acta Biochim. Pol.* **2006**, *53* (4), 685–691.

(4) Noodleman, L.; Lovell, T.; Liu, T.; Himo, F.; Torres, R. A. Insights into Properties and Energetics of Iron-Sulfur Proteins from Simple Clusters to Nitrogenase. *Curr. Opin. Chem. Biol.* **2002**, *6* (2), 259–273.

(5) Hagen, W. R. EPR Spectroscopy of Iron-Sulfur Proteins. In *Advances in Inorganic Chemistry, Iron-Sulfur Proteins*; Academic Press, Inc.: San Diego, 1992; pp 165–222.

(6) Guigliarelli, B.; Bertrand, P. Application of EPR Spectroscopy to the Structural and Functional Study of Iron-Sulfur Proteins. *Adv. Inorg. Chem.* **1999**, *47*, 421–497.

(7) Orio, M.; Mouesca, J.-M. Variation of Average *g* Values and Effective Exchange Coupling Constants among [2Fe−2S] Clusters: A Density Functional Theory Study of the Impact of Localization (Trapping Forces) versus Delocalization (Double-Exchange) as Competing Factors. *Inorg. Chem.* **2008**, *47* (12), 5394–5416.

(8) Bertrand, P.; Guigliarelli, B.; Gayda, J.-P.; Peter, B.; Gibson, J. F. A Ligand-Field Model to Describe a New Class of 2Fe-2S Clusters in Proteins and Their Synthetic Analogues. *Biochim. Biophys. Acta - Protein Struct. Mol. Enzymol.* **1985**, *831* (2), 261–266.

(9) Hagen, W. R.; Hearsen, D. O.; H, S. R.; Dunham, W. R.; Hearshen, D. O.; Sands, R. H.; Dunham, W. R. A Statistical Theory for Powder EPR in Distributed Systems. *J. Magn. Reson.* **1985**, *61* (2), 220–232.

(10) Hearshen, D. O.; Hagen, W. R.; Sands, R. H.; Grande, H. J.; Crespi, H. L.; Gunsalus, I. C.; Dunham, W. R. An Analysis of *g* Strain in the EPR of Two [2Fe-2S] Ferredoxins. Evidence for a Protein Rigidity Model. *J. Magn. Reson.* **1986**, *69* (3), 440–459.

(11) Abragam, A.; Bleaney, B. *Electron Paramagnetic Resonance of Transition Ions*; Marshall, W., Wilkinson, D. H., Eds.; Clarendon Press: Oxford, 1970.

(12) Bertrand, P.; Gayda, J. P.; Fee, J. A.; Kuila, D.; Cammack, R. Comparison of the Spin-Lattice Properties of the Two Classes of [2Fe-2S] Clusters in Proteins. *Biochim. Biophys. Acta* **1987**, *916*, 24–28.

(13) Gayda, J.-P.; Bertrand, P.; Deville, A.; More, C.; Roger, G.; Gibson, J. F.; Cammack, R. Temperature Dependence of the Electronic Spin-Lattice Relaxation Time in a 2-Iron-2-Sulfur Protein. *Biochim. Biophys. Acta* **1979**, *581*, 15–26.

(14) Gayda, J.-P.; Gibson, J. F.; Cammack, R.; Hall, D. O.; Mullinger, R. Spin Lattice Relaxation and Exchange Interaction in a 2-Iron, 2-Sulphur Protein. *Biochim. Biophys. Acta* **1976**, *434*, 154–163.

(15) Fielding, A. J.; Fox, S.; Milihauser, G. L.; Chattopadhyay, M.; Kroneck, P. M.; Fritz, G.; Eaton, G.; Eaton, S. S. Electron Spin Relaxation of copper(II) Complexes in Glassy Solution between 10 and 120K. *J. Magn. Res.* **2006**, *179*, 92–104.

(16) Sato, H.; Kathirvelu, V.; Fielding, A. J.; Blinco, J. P.; Micallef, A. S.; Bottle, S. E.; Eaton, S. S.; Eaton, G. R. Impact of Molecular Size on Electron Spin Relaxation Rates of Nitroxyl Radicals in Glassy Solvents between 100 and 300 K. *Mol. Phys.* **2007**, *105*, 2137–2151.

(17) Eaton, S. S.; Eaton, G. R. *Biological Magentic Resonance 19, Distance Measurement in Biological Systems by EPR*; Berliner, L. J., Eaton, S. S., Eaton, Gareth, R., Eds.; Kluwer Academic Publishers: New York, 2002.

(18) Bertrand, P.; Gayda, J.; Rao, K. K. Electron Spin–lattice Relaxation of the (4Fe–4S) Ferredoxin from *B. Stearothermophilus*. Comparison with Other Iron Proteins. *J. Chem. Phys.* **1982**, *76*

(10), 4715–4719.

(19) Berry, E. A.; Guergova-Kuras, M.; Huang, L.; Crofts, A. R. Structure and Function of Cytochrome *bc* Complexes. *Annu. Rev. Biochem.* **2000**, *69*, 1005–1075.

(20) Berry, E. A.; Huang, L.-S.; Saechao, L. K.; Pon, N. G.; Valkova-Valchanova, M.; Daldal, F. X-Ray Structure of *Rhodobacter Capsulatus* Cytochrome bc_1: Comparison with Its Mitochondrial and Chloroplast Counterparts. *Photosynth. Res.* **2004**, *81* (3), 251–275.

(21) Sarewicz, M.; Osyczka, A. Electronic Connection Between the Quinone and Cytochrome *c* Redox Pools and Its Role in Regulation of Mitochondrial Electron Transport and Redox Signaling. *Physiol. Rev.* **2015**, *95* (1), 219–243.

(22) Zhang, Z.; Huang, L.; Shulmeister, V. M.; Chi, Y. I.; Kim, K. K.; Hung, L. W.; Crofts, a R.; Berry, E. A.; Kim, S. H. Electron Transfer by Domain Movement in Cytochrome bc_1. *Nature* **1998**, *392* (6677), 677–684.

(23) Darrouzet, E.; Valkova-Valchanova, M.; Moser, C. C.; Dutton, P. L.; Daldal, F. Uncovering the [2Fe2S] Domain Movement in Cytochrome bc_1 and Its Implications for Energy Conversion. *Proc. Natl. Acad. Sci. U. S. A.* **2000**, *97* (9), 4567–4572.

(24) Darrouzet, E.; Moser, C. C.; Dutton, P. L.; Daldal, F. Large Scale Domain Movement in Cytochrome bc_1: A New Device for Electron Transfer in Proteins. *Trends in Biochem. Sci.* **2001**, *26* (7), 445–451.

(25) Cooley, J. W.; Roberts, A. G.; Bowman, M. K.; Kramer, D. M.; Daldal, F. The Raised Midpoint Potential of the [2Fe2S] Cluster of Cytochrome bc_1 Is Mediated by Both the Q_o Site Occupants and the Head Domain Position of the Fe-S Protein Subunit. *Biochemistry* **2004**, *43* (8), 2217–2227.

(26) Sarewicz, M.; Dutka, M.; Froncisz, W.; Osyczka, A. Magnetic Interactions Sense Changes in Distance between Heme b_L and the Iron-Sulfur Cluster in Cytochrome bc_1. *Biochemistry* **2009**, *48*, 5708–5720.

(27) Darrouzet, E.; Valkova-Valchanova, M.; Daldal, F. Movement of the Iron-Sulfur Subunit beyond the *ef* Loop of Cytochrome *b* Is Required for Multiple Turnovers of the bc_1 Complex but Not for Single Turnover Q_o Site Catalysis. *J. Biol. Chem.* **2002**, *277* (5), 3471–3476.

(28) Cooley, J. W.; Ohnishi, T.; Daldal, F. Binding Dynamics at the Quinone Reduction (Q_i) Site Influence the Equilibrium Interactions of the Iron Sulfur Protein and Hydroquinone Oxidation (Q_o) Site of the Cytochrome bc_1 Complex. *Biochemistry* **2005**, *44* (31), 10520–10532.

(29) Sarewicz, M.; Borek, A.; Cieluch, E.; Świerczek, M.; Osyczka, A. Discrimination between Two Possible Reaction Sequences That Create Potential Risk of Generation of Deleterious Radicals by Cytochrome bc_1. Implications for the Mechanism of Superoxide Production. *Biochim. Biophys. Acta* **2010**, *1797* (11), 1820–1827.

(30) Daldal, F.; Davidson, E.; Cheng, S. Isolation of the Structural Genes for the Rieske Fe-S Protein, Cytochrome *b* and Cytochrome c_1 All Components of the Ubiquinol: Cytochrome c_2 Oxidoreductase Complex of *Rhodopseudomonas Capsulata*. *J. Mol. Biol.* **1987**, *195*, 1–12.

(31) Atta-Asafo-Adjei, E.; Daldal, F. Size of the Amino Acid Side Chain at Position 158 of Cytochrome *b* is Critical for an Active Cytochrome bc_1 complex and for photosynthetic growth of *Rhodobacter capsulatus*. *Proc. Natl. Acad. Sci. U. S. A.* **1991**, *88* (2), 492–496.

(32) Valkova-Valchanova, M. B.; Saribas, A. S.; Gibney, B. R.; Dutton, P. L.; Daldal, F. Isolation and Characterization of a Two-Subunit Cytochrome *b*-c_1 Subcomplex from *Rhodobacter*

Capsulatus and Reconstitution of Its Ubihydroquinone Oxidation (Q_o) Site with Purified Fe-S Protein Subunit. *Biochemistry* **1998**, *37* (10), 16242–16251.

(33) Czapla, M.; Borek, A.; Sarewicz, M.; Osyczka, A. Enzymatic Activities of Isolated Cytochrome bc_1-like Complexes Containing Fused Cytochrome *b* Subunits with Asymmetrically Inactivated Segments of Electron Transfer Chains. *Biochemistry* **2012**, *51* (4), 829–835.

(34) Williams-Smith, D. L.; Bray, R. C.; Barber, M. J.; Tsopanakis, A. D.; Vincent, S. P. Changes in Apparent pH on Freezing Aquenous Buffer Solutions and Their Relevance to Biochemical Electron-Paramagnetic-Resonance Spectroscopy. *Biochem. J.* **1977**, *167*, 593–600.

(35) Pietras, R.; Sarewicz, M.; Osyczka, A. Molecular Organization of Cytochrome c_2 near the Binding Domain of Cytochrome bc_1 Studied by Electron Spin-Lattice Relaxation Enhancement. *J. Phys. Chem. B* **2014**, *118*, 6634–6643.

(36) Lindsey, C. P.; Patterson, G. D. Detailed Comparison of the Williams-Watts and Cole-Davidson Functions. *J. Chem. Phys.* **1980**, *73* (7), 3348–3357.

(37) Hagen, W. *Biomolecular EPR Spectroscopy*; CRC Press Taylor & Francis Group: Boca Raton, 2009.

(38) Thompson, P.; Cox, D. E.; Hastings, J. B. Rietveld Refinement of Debye-Scherrer Synchrotron X-Ray Data from Al_2O_3. *J. Appl. Crystallogr.* **1987**, *20* (2), 79–83.

(39) Ida, T.; Ando, M.; Toraya, H. Extended Pseudo-Voigt Function for Approximating the Voigt Profile. *J. Appl. Crystallogr.* **2000**, *33*, 1311–1316.

(40) D. Wang, G. H. A New Method for Simulating Randomly Oriented Powder Spectra in Magnetic Resonance: The Sydney Opera House (SOPHE) Method. *J. Magn. Reson. Ser. A* **1995**, *117*, 1–8.

(41) Ponti, A. Simulation of Magnetic Resonance Static Powder Lineshapes: A Quantitative Assessment of Spherical Codes. *J. Magn. Reson.* **1999**, *138* (2), 288–297.

(42) Hoffmann, S. K.; Hilczer, W.; Goslar, J.; Massa, M. M.; Calvo, R. Electron Spin Relaxation in Pseudo-Jahn-Teller Low-Symmetry Cu(II) Complexes in Diaqua(L-Aspartate)Zn(II)·H_2O Crystals. *J. Magn. Reson.* **2001**, *153* (1), 92–102.

(43) Nett, J.; Hunte, C.; Trumpower, B. L. Changes to the Length of the Flexible Linker Region of the Rieske Protein Impair the Interaction of Ubiquinol with the Cytochrome bc_1 Complex. *Eur. J. Biochem*. **2000**, *267*, 5777–5782.

(44) Borek, A.; Sarewicz, M.; Osyczka, A. Movement of the Iron-Sulfur Head Domain of Cytochrome bc_1 Transiently Opens the Catalytic Q_o Site for Reaction with Oxygen. *Biochemistry* **2008**, *47* (47), 12365–12370.

(45) Schroter, T.; Hatzfeld, O. M.; Gemeinhardt, S.; Korn, M.; Firedrich, T.; Ludwig, B.; Link, T. A. Mutational Analysis of Residues Forming Hydrogen Bonds in the Rieske [2Fe-2S] Cluster of the Cytochrome bc_1 Complex in *Paracoccus Denitrificans*. *Eur. J. Biochem.* **1998**, *255*, 100–106.

(46) Kolling, D. J.; Brunzelle, J. S.; Lhee, S.; Crofts, A. R.; Nair, S. K. Atomic Resolution Structures of Rieske Iron-Sulfur Protein: Role of Hydrogen Bonds in Tuning the Redox Potential of Iron-Sulfur Clusters. *Structure* **2007**, *15*, 29–38.

(47) Leggate, E. J.; Hirst, J. Roles of the Disulfide Bond and Adjacent Residues in Determining the Reduction Potentials and Stabilities of Respiratory-Type Rieske Clusters. *Biochemistry* **2005**, *44* (18), 7048–7058.

(48) Guergova-Kuras, M.; Kuras, R.; Ugulava, N.; Hadad, I.; Crofts, A. R. Specific Mutagenesis of the Rieske Iron−Sulfur Protein in *Rhodobacter Sphaeroides* Shows That Both the Thermodynamic Gradient and the pK of the Oxidized Form Determine the Rate of Quinol Oxidation by the bc_1 Complex. *Biochemistry* **2000**, *39* (25), 7436–7444.

(49) Denke, E.; Merbitz-Zahradnik, T.; Hatzfeld, O. M.; Snyder, C. H.; Link, T. A.; Trumpower, B. L. Alteration of the Midpoint Potential and Catalytic Activity of the Rieske Iron-Sulfur Protein by Changes of Amino Acids Forming Hydrogen Bonds to the Iron-Sulfur Cluster. *J. Biol. Chem.* **1998**, *273* (15), 9085–9093.

(50) Shinkarev, V. P.; Kolling, D. R. J.; Miller, T. J.; Crofts, A. R. Modulation of the Midpoint Potential of the [2Fe-2S] Rieske Iron Sulfur Center by Q_o Occupants in the bc_1 Complex. *Biochemistry* **2002**, *41* (48), 14372–14382.

(51) Kuznetsov, A. M.; Zueva, E. M.; Masliy, A. N.; Krishtalik, L. I. Redox Potential of the Rieske Iron–sulfur Protein: Quantum-chemical and Electrostatic Study. *Biochim. Biophys. Acta* **2010**, *1797* (3), 347–359.

(52) Esser, L.; Quinn, B.; Li, Y.-F.; Zhang, M.; Elberry, M.; Yu, L.; Yu, C.-A.; Xia, D. Crystallographic Studies of Quinol Oxidation Site Inhibitors: A Modified Classification of Inhibitors for the Cytochrome bc_1 Complex. *J. Mol. Biol.* **2004**, *341* (1), 281–302.

(53) Von Jagow, G.; Link, T. A. Use of Specific Inhibitors on the Mitochondrial bc_1 Complex. *Methods Enzymol.* **1986**, *126*, 253–271.

(54) Berry, E. A.; Huang, L.-S. Conformationally Linked Interaction in the Cytochrome bc_1 Complex between Inhibitors of the Q_o Site and the Rieske Iron-Sulfur Protein. *Biochim. Biophys. Acta* **2011**, *1807* (10), 1349–1363.

(55) Kessl, J. J.; Lange, B. B.; Merbitz-Zahradnik, T.; Zwicker, K.; Hill, P.; Meunier, B.; Palsdottir, H.; Hunte, C.; Meshnick, S.; Trumpower, B. L. Molecular Basis for Atovaquone Binding to the Cytochrome bc_1 Complex. *J. Biol. Chem.* **2003**, *278* (33), 31312–31318.

(56) Nayak, S. K.; Mallik, S. B.; Kanaujia, S. P.; Sekar, K.; Ranganathan, K. R.; Ananthalakshmi, V.; Jeyaraman, G.; Saralaya, S. S.; Rao, K. S.; Shridhara, K.; et al. Crystal Structures and Binding Studies of Atovaquone and Its Derivatives with Cytochrome bc_1: A Molecular Basis for Drug Design. *CrystEngComm* **2013**, *15* (24), 4871–4884.

(57) Barton, V.; Fisher, N.; Biagini, G. A.; Ward, S. A.; O'Neill, P. M. Inhibiting *Plasmodium* Cytochrome bc_1: A Complex Issue. *Curr. Opin. Chem. Biol.* **2010**, *14* (4), 440–446.

(58) Gao, X.; Wen, X.; Yu, C. C.-A.; Esser, L.; Tsao, S.; Quinn, B.; Zhang, L.; Yu, L.; Xia, D. The Crystal Structure of Mitochondrial Cytochrome bc_1 in Complex with Famoxadone: The Role of Aromatic-Aromatic Interaction in Inhibition. *Biochemistry* **2002**, *41* (39), 11692–11702.

(59) Muller, F. L.; Roberts, A. G.; Bowman, M. K.; Kramer, D. M. Architecture of the Q_o Site of the Cytochrome bc_1 Complex Probed by Superoxide Production. *Biochemistry* **2003**, *42* (21), 6493–6499.

(60) Bertini, I.; Ciurli, S.; Luchinat, C.; Capponi, V. G.; Pichat, V. B.; Distribution, V. The Electronic Structure of FeS Centers in Proteins and Models a Contribution to the Understanding of Their Electron Transfer Properties. *Struct. Bond.* **1995**, *83*, 1–53.

(61) Fiethen, S. A.; Staemmler, V.; Nair, N. N.; Ribas-Arino, J.; Schreiner, E.; Marx, D. Revealing the Magnetostructural Dynamics of [2Fe-2S] Ferredoxins from Reduced-Dimensionality Analysis of Antiferromagnetic Exchange Coupling Fluctuations. *J. Phys. Chem. B* **2010**, *114* (35), 11612–11619.

(62) Zhou, Y.; Bowler, B. E.; Eaton, G. R.; Eaton, S. S. Electron Spin Lattice Relaxation Rates for S= 1/2 Molecular Species in Glassy Matrices or Magnetically Dilute Solids at Temperatures between 10 and 300 K. *J. Magn. Reson.* **1999**, *174*, 165–174.

(63) Usselman, R. J.; Fielding, A. J.; Frerman, F. E.; Watmough, N. J.; Eaton, G. R.; Eaton, S. S.; Simkovic, M. Impact of Mutations on the Midpoint Potential of the [4Fe-4S]+ 1,+2 Cluster and on Catalytic Activity in Electron Transfer Flavoprotein-Ubiquinone Oxidoreductase (ETF-QO). *Biochemistry* **2008**, *47* (1), 92–100.

(64) Iwata, S.; Lee, J. W.; Okada, K.; Lee, J. K.; Iwata, M.; Rasmussen, B.; Link, T. A.; Ramaswamy, S.; Jap, B. K. Complete Structure of the 11-Subunit Bovine Mitochondrial Cytochrome bc_1 Complex. *Science* **1998**, *281* (July), 64–71.

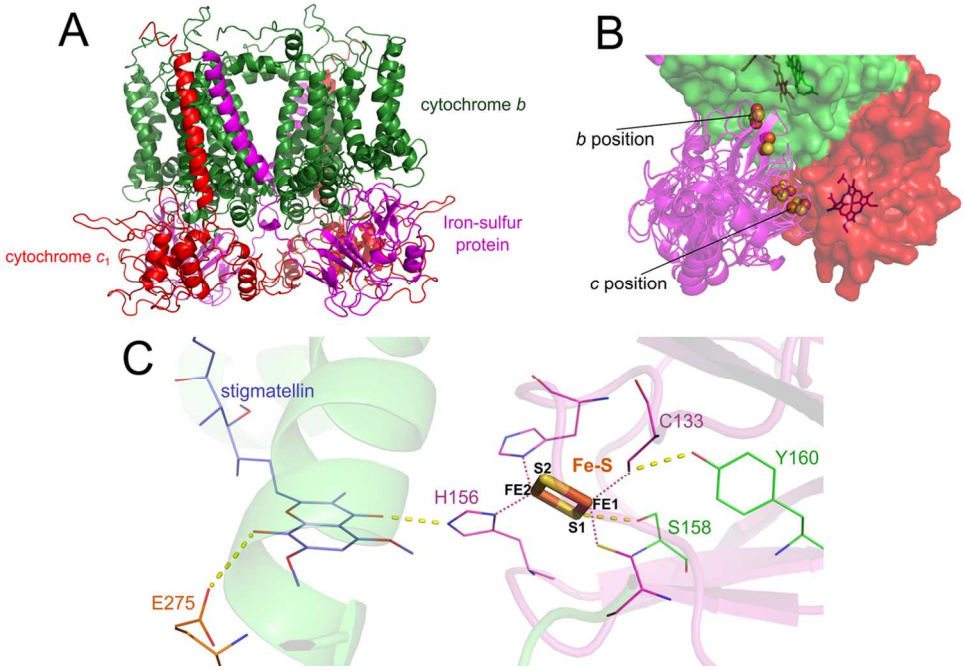

113x75mm (300 x 300 DPI)

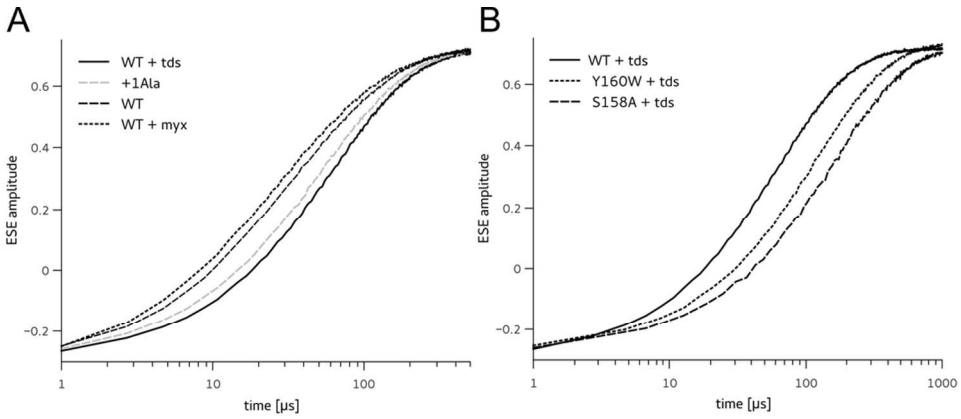

101x42mm (300 x 300 DPI)

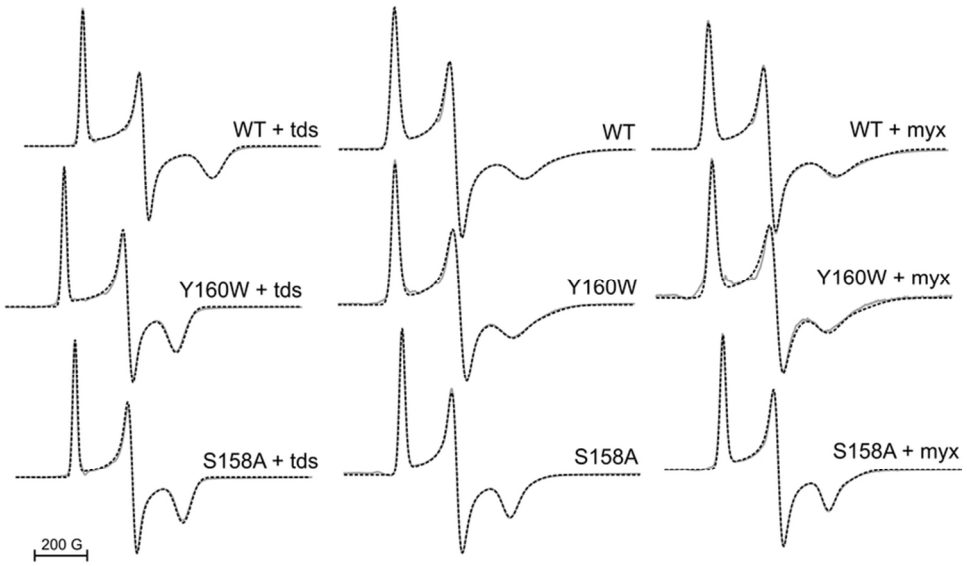

80x45mm (300 x 300 DPI)

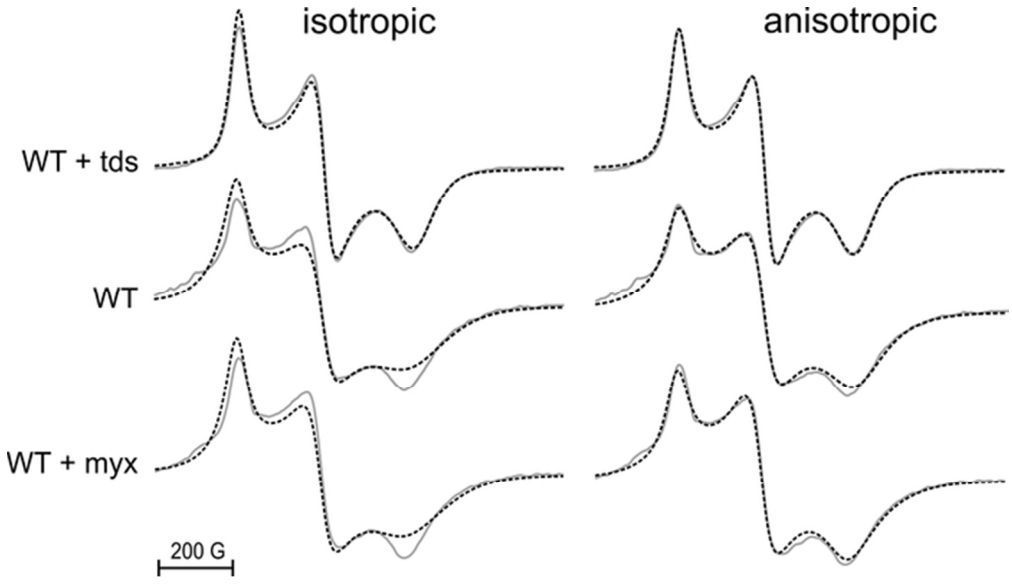

58x33mm (300 x 300 DPI)

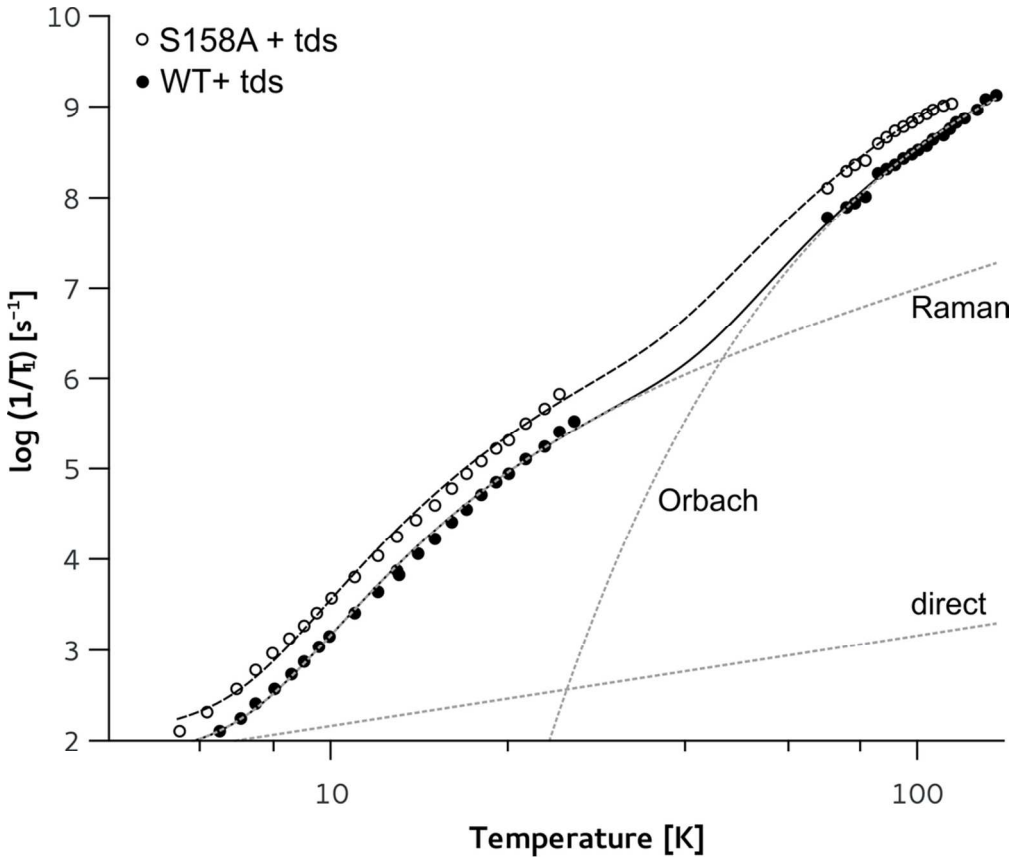

94x80mm (300 x 300 DPI)

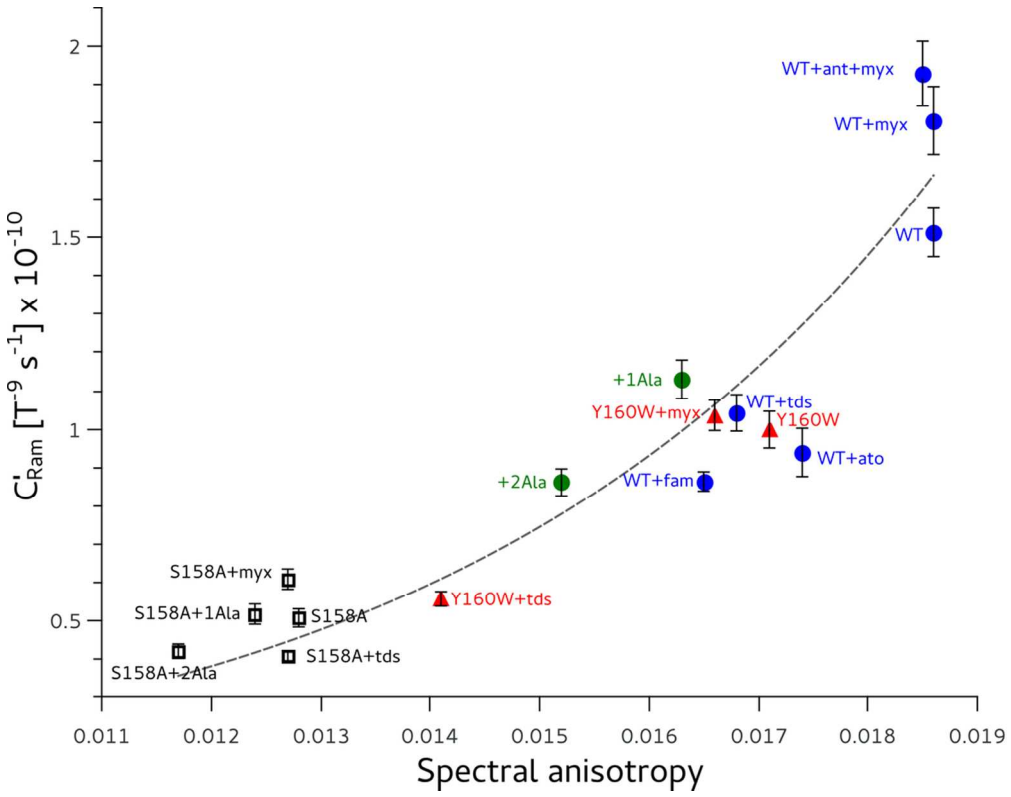

99x77mm (300 x 300 DPI)